

中国激光

双孔点衍射干涉成像系统波像差检测技术研究

冯鹏^{1,2}, 唐峰^{1,2*}, 王向朝^{1,2}, 卢云君^{1,2}, 徐静浩¹, 郭福东¹, 张国先¹

¹ 中国科学院上海光学精密机械研究所信息光学与光电技术实验室, 上海 201800;

² 中国科学院大学材料与光电研究中心, 北京 100049

摘要 提出了一种用于测量高精度成像系统的双孔点衍射干涉仪, 具有高光场均匀性、高可测量数值孔径、准共光路、相移元件在系统成像光路以外的优点。设计了两种测量模式, 点衍射测量模式和系统误差测量模式, 其中系统误差模式用于标定干涉仪的系统误差。分别搭建了双孔点衍射干涉和双光纤点衍射干涉的实验装置, 完成了对设计波像差小于 0.045λ RMS, $5\times$ 透射式投影物镜的检测实验。实验结果表明, 与双光纤点衍射干涉仪对比, 双孔点衍射的波像差测量相对误差为 0.07 nm RMS , 且干涉图具有更加良好的光强均匀性。验证了本文检测技术的有效性。

关键词 测量; 点衍射; 针孔点衍射; 波像差检测; 干涉测量

中图分类号 O436.1

文献标志码 A

doi: 10.3788/CJL202148.0904002

1 引言

波像差是评价光学系统成像质量的重要参数。高品质的显微物镜和空间望远镜的波像差需小于 $\lambda/14$ RMS (λ 为工作波长, RMS 为均方根值)^[1-3]。光刻投影物镜的波像差需达到 0.5 nm RMS 以下, 这对波像差检测技术提出了很高的要求^[4-5]。

现有的波前检测技术主要有夏克-哈特曼、菲索干涉、泰曼格林干涉、横向剪切干涉、点衍射干涉等。夏克-哈特曼传感器具有较大的测量范围, 能够快速测量波前, 但是它的采样点少, 空间分辨率不够^[6-7]。菲索干涉仪和泰曼格林干涉仪的测量精度均受限于标准镜头的精度, 干涉仪结构复杂、体积随被测物口径而倍增且不易于调整^[8-9]。横向剪切干涉技术利用被检面自身产生的双光束干涉, 不需要参考波面即可实现波前的实时测量, 但是要恢复原始波面需要两个垂直方向的剪切干涉图, 波前重构算法与哈特曼传感器方法一样, 较为复杂^[10]。点衍射干涉检测技术是利用针孔衍射光波作为参考波面, 从而摆脱了常用干涉仪中测量精度受实体标准镜精度的限制^[11-12]。点衍射干涉仪由 Smartt 首次提出, 而后 Medecki 提出了相移点衍射干涉仪, 利用相移法提

高了测量精度^[13-14], 国内王晨等^[15]做了偏振相移动点衍射干涉技术方面的工作。美国的伯克利实验室利用相移点衍射干涉仪测量极紫外光刻投影物镜波像差, 其测量重复性达到 0.1 nm RMS ^[16-20]。中国科学院上海光学精密机械研究所提出了一种双光纤点衍射干涉仪 (DFPDI), 利用单模光纤产生近似球面波^[21]。但是芯径小于 $2\mu\text{m}$ 的光纤很难制作, 单模光纤衍射光数值孔径小且光强呈类高斯分布, 导致干涉图样的光强中心强边缘弱, 影响光瞳边缘的检测精度。

本文提出了一种基于双光纤光路的双孔点衍射干涉 (DHPDI) 成像系统波像差检测技术及其系统误差的标定方法。利用针孔衍射产生理想球面波, 可达到较大出射数值孔径, 能够获得高对比度且光强均匀的干涉图样。搭建实验装置对成像系统进行波像差检测, 实验结果及比对测量结果验证了理论推导的有效性。

2 双孔点衍射干涉仪检测原理

图 1 为本文所提出双孔点衍射干涉仪的测量原理图。光源采用短相干, 波长为 532 nm 的激光器。激光器输出光被分束器分为两束, 形成准共光路干

收稿日期: 2020-11-09; 修回日期: 2020-12-06; 录用日期: 2020-12-21

*E-mail: tangfeng@siom.ac.cn

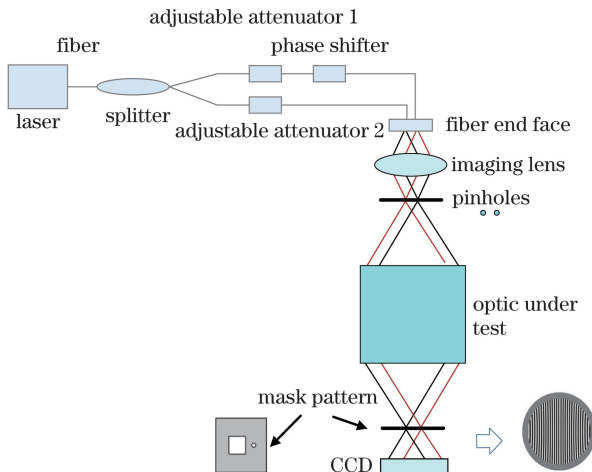


图 1 双孔点衍射干涉仪测量原理图

Fig. 1 Measuring principle of double-hole point diffraction interferometer

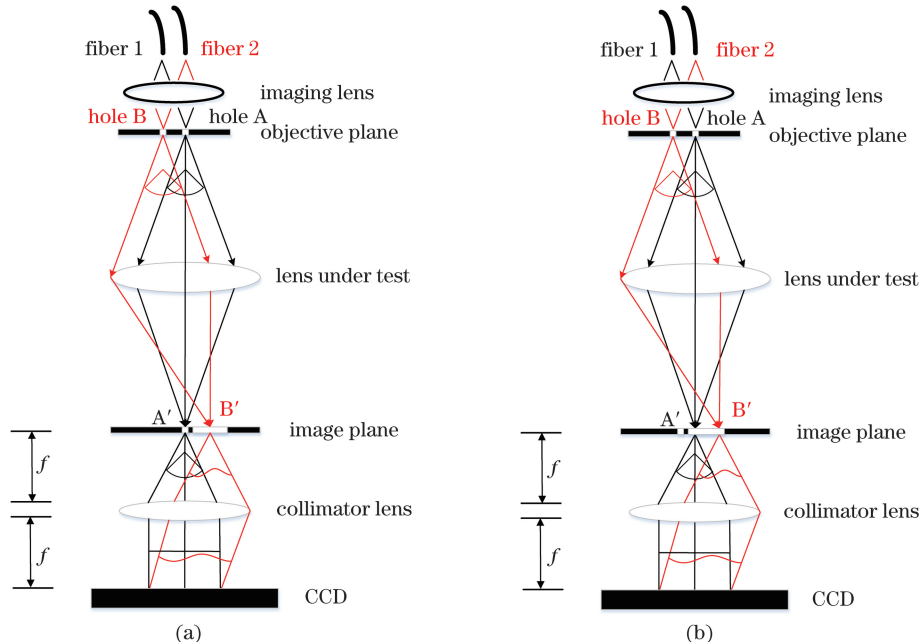


图 2 系统误差标定图。(a)点衍射测量模式,(b)系统误差测量模式

Fig. 2 Schematic diagram of system errors calibration. (a) Point diffraction measurement mode; (b) system errors measurement mode

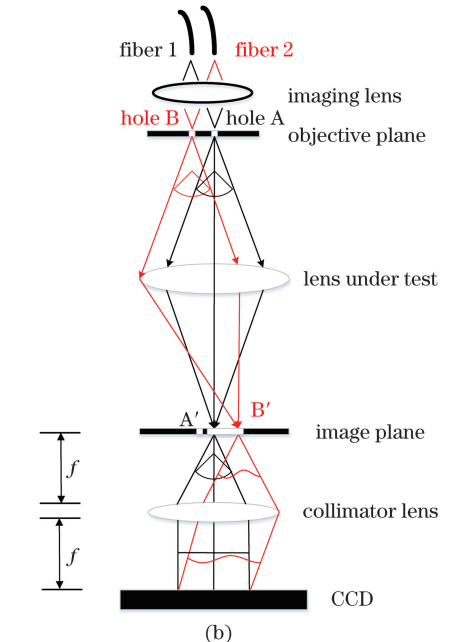
3 干涉仪系统误差标定

本干涉仪设计了两种测量模式:点衍射测量模式和系统误差测量模式。在点衍射测量模式中,测量结果包含了测试光和点衍射光的几何光程误差、探测器倾斜误差,主要表现为彗差、像散(与实验结果一致)^[22-23]。通过系统误差模式测量,可以快速方便地标定这些几何光程差。两种测量模式配合使用,能够高精度地检测被测成像系统的波像差。

图 2(a)为点衍射测量模式的测量原理图。通过这种模式可以得到数据 W_m , 表示为

涉仪结构。两路干涉臂均接有可调衰减器可分别控制其光强,其中一路干涉臂还接有相移器。

如图 2 所示,物面的单模光纤 1 和单模光纤 2 输出两束相干光,其端面被透镜成像于物面掩模板的针孔 A 和针孔 B 处,被针孔滤波形成两个标准球面波照明被测成像系统。两个波前分别作为测量波前和参考波前通过待测成像系统,针孔 A 和针孔 B 经待测成像系统成像于其像面 A' 和 B' 处。一束光通过像面掩模板上的针孔,另外一束光通过像面掩模板上的光窗形成点衍射测量模式;两束光均通过像面掩模板上的光窗形成系统误差测量模式。两束光经过像面掩模板,空间会合后在 CCD 表面形成干涉条纹,CCD 采集相移干涉图,再经计算机软件图像处理,得到被测成像系统的波像差信息。



$$W_m = \Delta L - W_{\text{pinhole}} + W_{\text{HoleB}} + W_{\text{lensB}}, \quad (1)$$

式中: ΔL 为两束干涉光分别通过像面掩模衍射小孔和光窗后的几何光程差; W_{pinhole} 为光束通过像面掩模针孔的衍射波前误差; W_{HoleB} 为光束经过物面针孔 B 的衍射波前误差; W_{lensB} 为被测成像物镜的波像差。

图 2(b)为系统误差测量模式的测量原理图。利用双窗像面掩模代替孔窗掩模即可测量得到数据 W_s , 表示为

$$W_s = \Delta L - W_{\text{HoleA}} - W_{\text{lensA}} + W_{\text{HoleB}} + W_{\text{lensB}}, \quad (2)$$

式中: ΔL 为两束干涉光通过像面光窗后的几何光程差; W_{HoleA} 为光束经过物面针孔A的衍射波前误差; W_{lensA} 为被测成像物镜的波像差; W_{HoleB} 为光束经过物面小孔B的衍射波前误差; W_{lensB} 为被测成像物镜的波像差。

将点衍射测量结果 W_m 减去系统误差测量结果 W_s ,可以得到

$$\begin{aligned} W = & W_m - W_s = \\ & \Delta L - W_{\text{pinhole}} + W_{\text{HoleB}} + W_{\text{lensB}} - \\ & (\Delta L - W_{\text{HoleA}} - W_{\text{lensA}} + W_{\text{HoleB}} + W_{\text{lensB}}) = \\ & W_{\text{lensA}} + W_{\text{HoleA}} - W_{\text{pinhole}}. \end{aligned} \quad (3)$$

从(3)式可以看出,计算得到的结果 W 中除了成像系统的波像差之外,还包含有物面针孔A产生的衍射波前误差 W_{HoleA} 和像面针孔产生的衍射波前误差 W_{pinhole} 。通过时域有限差分(FDTD)方法仿真,得到 W_{HoleA} 在工作波长 $\lambda=532\text{ nm}$ 、小孔直径为700 nm、数值孔径为0.06时,衍射波面偏差小于 $\lambda/10^5$ RMS; W_{pinhole} 在工作波长 $\lambda=532\text{ nm}$ 、小孔直径为700 nm、数值孔径为0.3时,衍射波面偏差小于 $\lambda/10^4$ RMS。由下式估算,该干涉仪的测量不确定度 $\mu_{\text{dh}}(w)$ 可达到 $\lambda/10^4$ RMS。

$$\mu_{\text{dh}}(w) = \sqrt{\mu^2(w_{\text{HoleA}}) + \mu^2(w_{\text{pinhole}})}. \quad (4)$$

若双孔点衍射干涉仪去除物面成像透镜及物面小孔,光纤直接照明待测成像系统,其余不变,即成为双光纤点衍射干涉仪^[18],采用与双孔点衍射干涉仪相同的系统误差标定方法,其测量结果 W_{df} 表示为

$$W_{\text{df}} = W_{\text{lensA}} + W_{\text{Fiberl}} - W_{\text{pinhole}}. \quad (5)$$

从(5)式可以看出,测量结果中除了投影物镜波像差以外,还包含了物面光纤的衍射波前误差 W_{Fiberl} 和像面针孔产生的衍射波前误差 W_{pinhole} ,通过FDTD方法仿真,物面单模光纤芯径为2 μm、数值孔径为0.06时,衍射波面偏差小于 $\lambda/10^4$ RMS, W_{pinhole} 在工作波长 $\lambda=532\text{ nm}$ 、小孔直径为700 nm、数值孔径为0.3时,衍射波面偏差小于 $\lambda/10^4$ RMS。双光纤点衍射干涉仪的测量不确定度 $\mu_{\text{df}}(w)$ 可以由下式估算,可达到 $1.42\lambda/10^4$ RMS。

$$\mu_{\text{df}}(w) = \sqrt{\mu^2(w_{\text{Fiberl}}) + \mu^2(w_{\text{pinhole}})}. \quad (6)$$

4 实验

4.1 双孔点衍射干涉实验

本文搭建了双孔点衍射干涉测量装置,被测物镜为5×透射式显微物镜,像方 $NA=0.3$,物方

$NA=0.06$,设计波像差RMS小于 0.045λ 。实验使用工作波长为532 nm、相干长度约厘米量级、输出光功率30 mW的多纵模固体激光器;可调衰减器分辨率为0.01%;物面光纤采用芯径为2 μm的单模光纤。物面和像面掩模板均采用硅为基底,覆盖有200 nm SiN膜和500 nm Cr膜的遮光层。物面掩模板针孔直径为700 nm;像面掩模板针孔直径为700 nm,光窗尺寸为 $100\text{ }\mu\text{m}\times 100\text{ }\mu\text{m}$ 。为了实现较高的测量重复性,测量装置在真空中运行,采用真空中主动隔振系统进行系统隔振,系统具有良好的稳定性,采用连续36组波像差检测结果评估系统短期测量重复性^[24],单次测量(无平均)波面测试重复性达到50 pm RMS,满足测量重复性要求,因此本文实验数据均为单次测量结果。

图3(a)为双孔点衍射干涉系统误差干涉图,图3(b)为其点衍射测量干涉图。图4为投影物镜波像差测量结果及其Zernike 5~37项多项式拟合系数,其中图4(a)和图4(b)分别为去掉直流项、倾斜和离焦后的点衍射测量结果和系统误差测量结果,图4(c)为被测投影物镜的波像差检测Zernike 5~37项多项式拟合后的结果,其值为8.45 nm RMS。图4(a)的Zernike多项式拟合结果中,主要像差成分为Z7彗差215.89 nm,以及占较小比重的像散Z5 X轴向像散19.52 nm、Z6 Y轴向像散8.51 nm;图4(b)的Zernike多项式拟合结果中,主要像差成分为Z7彗差212.06 nm,以及占较小比重的像散Z5 X轴向像散23.41 nm、Z6 Y轴向像散6.12 nm;图4(c)波像差测量Zernike拟合结果中,Z7彗差-3.89 nm,像散Z5 X轴向像散3.83 nm、Z6 Y轴向像散-2.45 nm,已无明显彗差及像散成分,表明系统误差已被有效标定。

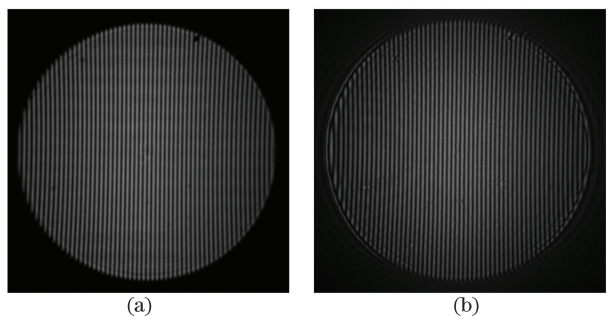


图3 双孔点衍射实验干涉图。(a) 系统误差干涉图;(b) 点衍射干涉图

Fig. 3 Interference diagrams in DHPDI experiment.
(a) System error interferogram; (b) point diffraction interferogram

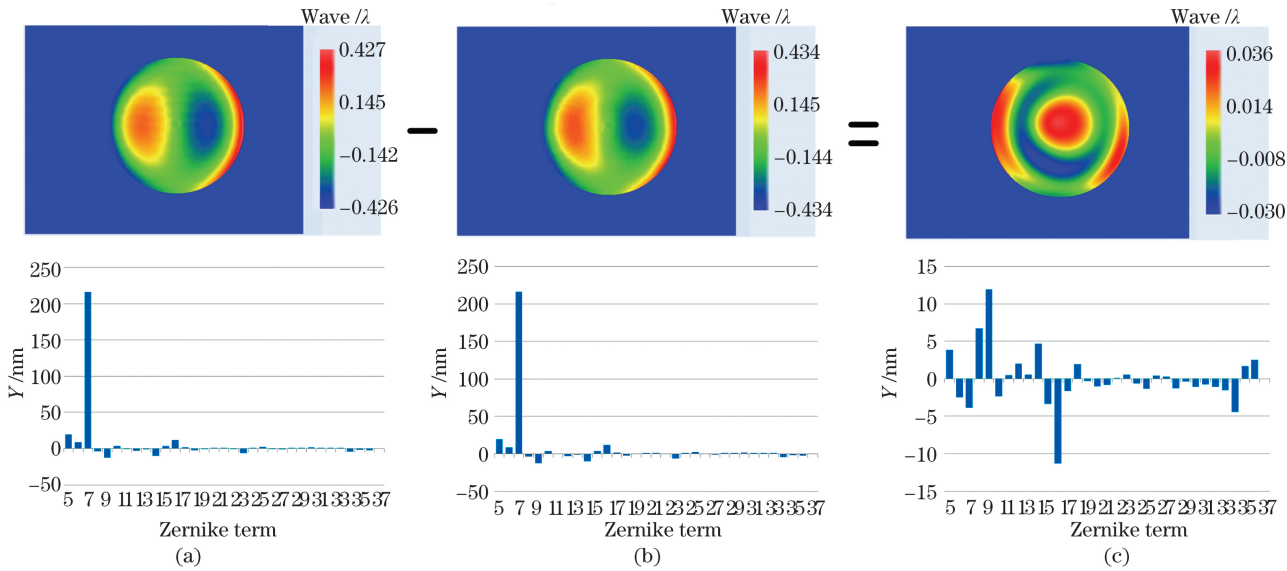


图4 投影物镜波像差测量结果及其5~37项Zernike多项式拟合系数。(a)系统误差测量结果,75.66 nm RMS;(b)点衍射测量结果,76.92 nm RMS;(c)波像差检测结果,8.45 nm RMS

Fig. 4 Wavefront aberration detection results of the measured objective lens and the 5~37 Zernike polynomials fitting.
(a) System error measurement results, 75.66 nm RMS; (b) point diffraction measurement results, 76.92 nm RMS;
(c) wave aberration detection results, 8.45 nm RMS

4.2 双光纤点衍射实验

本文还进行了双光纤点衍射干涉实验。在双孔点衍射实验条件下,除去物面成像透镜和带有针孔的物面掩模板,光纤直接照明被测成像系统,其余不变,即成为双光纤点衍射干涉仪^[21]。图5(a)为双光纤点衍射系统误差测量干涉图,图5(b)为其点衍射测量干涉图。图6为投影物镜波像差测量结果及其Zernike 5~37项多项式拟合系数,其中图6(a)和图6(b)为去掉直流项、倾斜和离焦后的点衍射测量结果和系统误差测量结果,图6(c)为被测投影物镜的波像差检测Zernike 5~37项多项式拟合后的结果,其值为8.52 nm RMS。图6(a)、图6(b)的Zernike多项式拟合结果中,主要像差成分为Z7彗

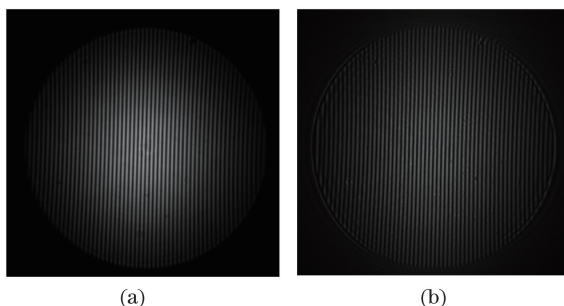


图5 双光纤点衍射实验干涉图。(a)系统误差测量结果图;(b)点衍射测量结果

Fig. 5 Interference diagrams in DFPDI experiment.
(a) System error measurement results; (b) point diffraction measurement results

差,以及占较小比重的像散Z5、Z6;图6(c)波像差测量Zernike拟合结果中已无明显彗差成分,表明系统误差已被有效标定。

4.3 实验对比及分析

图4为双孔点衍射干涉实验的投影物镜波像差测量结果,图6为双光纤点衍射干涉实验的投影物镜波像差测量结果。使用两种测量方法对同一投影物镜进行波像差检测,两者检测结果的波前分布近乎一致,相对误差为0.07 nm RMS(由于两次测量所在的视场点较难保证重合,因此没有采用数据像素相减的方式进行比较)。

图7为双孔点衍射和双光纤点衍射干涉两种测量模式下干涉图的光强分布及干涉对比度曲线,利用相移干涉图计算其中心位置X方向各像素点的光强及对比度,实线曲线代表双孔点衍射,虚线曲线代表双光纤点衍射。图7(a)为系统误差测量模式干涉图光强分布曲线图,其中双孔点衍射的光强非均匀性为34%,双光纤点衍射的光强非均匀性为77%;图7(b)为系统误差测量干涉图的对比度曲线图,其中双孔点衍射的干涉对比度为70%~75%,双光纤点衍射的干涉对比度为67%~72%;图7(c)为点衍射测量模式干涉图光强分布曲线图,其中双孔点衍射的光强非均匀性为48%,双光纤点衍射的光强非均匀性为60%;图7(d)为系统误差测量干涉图的对比度曲线图,其中双孔点衍射的干涉对比度

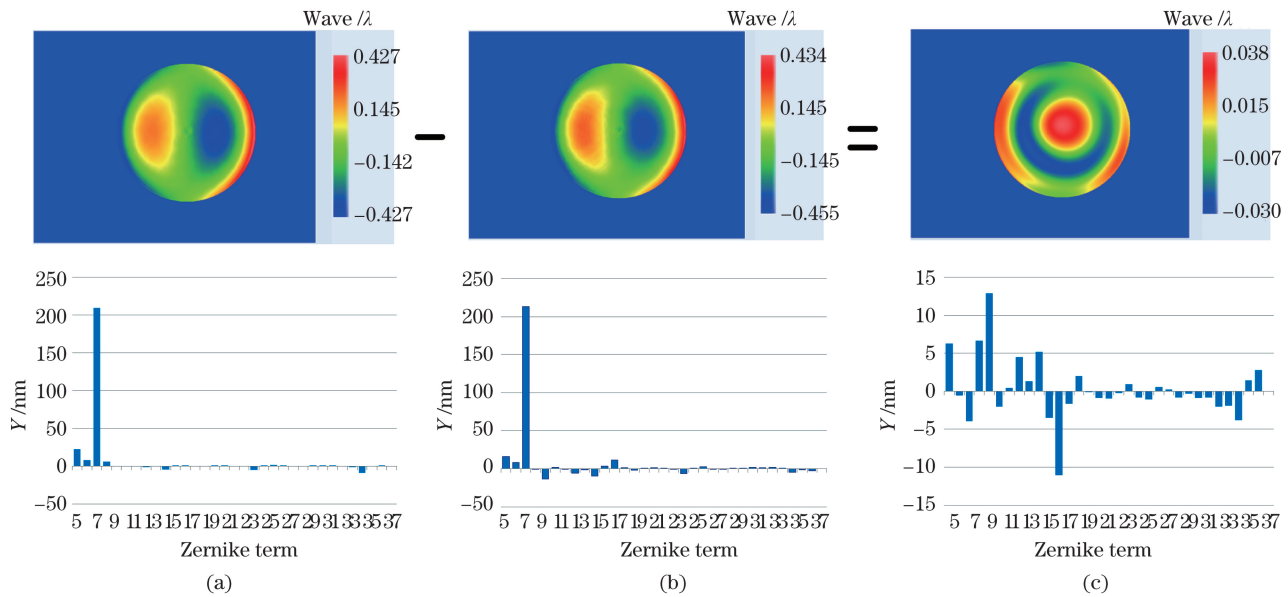


图6 投影物镜波像差测量结果及其5~37项Zernike多项式拟合系数。(a)系统误差测量结果,75.69 nm RMS;(b)点衍射测量结果,77.26 nm RMS;(c)波像差检测结果,8.52 nm RMS

Fig. 6 Wavefront aberration detection results of the measured objective lens and the 5–37 Zernike polynomials fitting.
(a) System error measurement results, 75.69 nm RMS; (b) point diffraction measurement results, 77.26 nm RMS;
(c) wave aberration detection results, 8.52 nm RMS

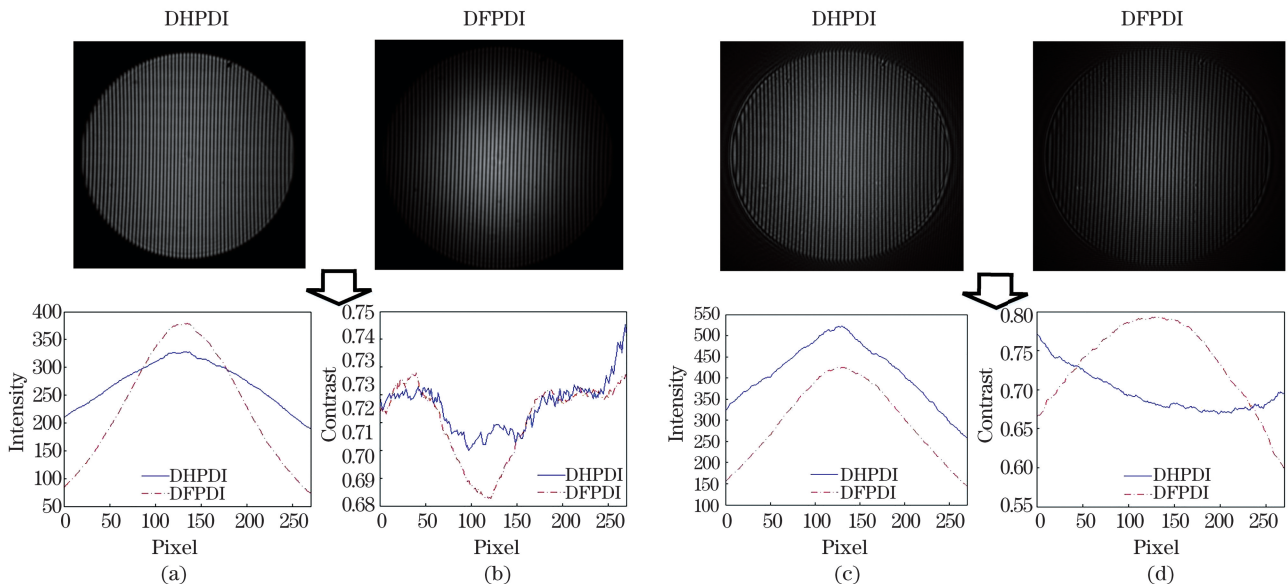


图7 两种测量模式下双孔点衍射干涉仪和双光纤点衍射干涉仪干涉图在X方向的光强分布及对比度曲线。(a)系统误差测量模式下两种干涉图的光强分布;(b)系统误差测量模式下两种干涉图的对比度分布;(c)点衍射测量模式下两种干涉图的光强分布;(d)点衍射测量模式下两种干涉图的对比度分布

Fig. 7 Intensity distribution and contrast curve of interferograms of the DHPDI and DFPDI in X direction under two measurement modes. (a) Intensity distribution of two kind of interferograms under the mode of system error measurement; (b) contrast curve of two kind of interferograms under the mode of system error measurement; (c) intensity distribution of two kind of interferograms under the mode of point diffraction measurement;
(d) contrast curve of two kind of interferograms under the mode of point diffraction measurement

为67%~77%，双光纤点衍射的干涉对比度为60%~79%。

实验结果表明，双孔点衍射干涉仪相对双光纤

点衍射干涉仪具有更好的光强均匀性，这是由于光纤出射NA相对较小(约0.1)，且光强分布呈高斯函数，因此在 $NA = 0.06$ 范围内光强均匀性较差，

且难以改变,而小孔衍射可以产生更高的出射NA,光强均匀性得到了改善;特别是光瞳边缘区域,双光纤点衍射干涉仪在光瞳边缘的光强只有中心光强的近30%,不利于提高光瞳边缘的检测精度;而双孔点衍射干涉仪在光瞳边缘的光强为区域中心的近80%,有助于提高光瞳边缘的检测精度。由于光强分布均匀性的提高,双孔点衍射干涉仪的干涉对比度一致性也相对双光纤点衍射干涉仪提高了约1倍。

5 结 论

本文研究了双孔点衍射干涉检测技术,物像面均采用直径700 nm的针孔产生标准球面波,其衍射波面偏差能够满足高精度成像系统波像差检测的要求。干涉仪采用全光纤光路传输,简化了干涉仪整体结构,且具有便捷调节干涉对比度及在成像光路之外产生相移的优点。

搭建了双孔点衍射干涉实验装置,同时搭建了双光纤点衍射干涉实验装置对同一投影物镜进行了比对测量。结果显示,双孔点衍射干涉仪两种模式下的干涉图对比度均优于65%;且其干涉图的光强均匀性比双光纤点衍射干涉提高了两倍,有利于提高光瞳边缘的检测精度。两者检测结果的波前分布相对误差小于0.1 nm RMS,验证了本文干涉仪检测技术的有效性。

参 考 文 献

- [1] Shirai T, Barnes T H, Haskell T G, et al. Adaptive wave-front correction by means of all-optical feedback interferometry[J]. Optics Letters, 2000, 25(11): 773-775.
- [2] Malacara D. Optical shop testing [M]. Hoboken: John Wiley & Sons, 2007.
- [3] Miyakawa R H. Wavefront metrology for high resolution optical systems [EB/OL]. [2020-11-09]. <https://search.proquest.com/docview/896620201>.
- [4] Liu K, Li Y Q. At-wavelength interferometry of projection optics for extreme ultraviolet lithography [J]. Chinese Journal of Lasers, 2009, 36(s2): 257-262.
- 刘克, 李艳秋. 极紫外光刻投影物镜波像差在线检测技术[J]. 中国激光, 2009, 36(s2): 257-262.
- [5] Ohmura Y, Tsuge Y, Hirayama T, et al. High-order aberration control during exposure for leading-edge lithography projection optics[J]. Proceedings of SPIE, 2016, 9780: 97800Y.
- [6] Shen F, Jiang W H. The measurement error of wavefront phase with shack-hartmann wavefront sensor[J]. Acta Optica Sinica, 2000, 20(5): 666-671.
- 沈锋, 姜文汉, 夏克-哈特曼波前传感器的波前相位探测误差[J]. 光学学报, 2000, 20(5): 666-671.
- [7] Dai X Y, Tan Y, Ren G, et al. Analysis of image quality detection performance of scanning hartmann technology[J]. Acta Optica Sinica, 2020, 40(7): 0712002.
- 戴勋义, 谭毅, 任戈, 等. 扫描哈特曼方法的像质检测性能分析[J]. 光学学报, 2020, 40(7): 0712002.
- [8] Howes W L. Lens collimation and testing using a Twyman-Green interferometer with a self-pumped phase-conjugating mirror[J]. Applied Optics, 1986, 25(4): 473-474.
- [9] Miao E L, Zhang J, Gu Y Q, et al. Measurement error analysis of high precision Fizeau interferometer for lithography projection objective [J]. Chinese Journal of Lasers, 2010, 37(8): 2029-2034.
- 苗二龙, 张健, 谷勇强, 等. 用于光刻投影物镜检测的高精度菲佐干涉仪误差分析[J]. 中国激光, 2010, 37(8): 2029-2034.
- [10] Li J, Tang F, Wang X Z, et al. System errors analysis of grating lateral shearing interferometer[J]. Chinese Journal of Lasers, 2014, 41(5): 0508006.
- 李杰, 唐峰, 王向朝, 等. 光栅横向剪切干涉仪及其系统误差分析[J]. 中国激光, 2014, 41(5): 0508006.
- [11] Chen X, Gramaglia M, Yeazell J A, et al. Phase-shifting interferometry with uncalibrated phase shifts [J]. Applied Optics, 2000, 39(4): 585-591.
- [12] Chen Y K, Li Y, Wang C, et al. Wavefront analysis method of pinhole point-diffraction based on waveguide theory[J]. Acta Optica Sinica, 2019, 39(11): 1112001.
- 陈元恺, 李瑶, 王晨, 等. 基于波导理论的针孔点衍射波前分析方法[J]. 光学学报, 2019, 39(11): 1112001.
- [13] Smartt R N, Strong J. Point-diffraction interferometer[J]. Journal of the Optical Society of America, 1974, 13(5): 198.
- [14] Medecki H, Tejnil E, Goldberg K A, et al. Phase-shifting point diffraction interferometer [J]. Optics Letters, 1996, 21(19): 1526-1528.
- [15] Wang C, Zhou Y, Lu Q, et al. Research on reflective polarization phase-shifting dynamic point diffraction interferometry[J]. Chinese Journal of Lasers, 2020, 47(10): 1004003.
- 王晨, 周游, 鲁棋, 等. 反射式偏振相移动态点衍射干涉技术的研究[J]. 中国激光, 2020, 47(10): 1004003.
- [16] Goldberg K A, Naulleau P P, Denham P E, et al.

- At-wavelength alignment and testing of the 0.3 NA MET optic [J]. Journal of Vacuum Science & Technology B: Microelectronics and Nanometer Structures, 2004, 22(6): 2956.
- [17] Naulleau P P, Goldberg K A, Lee S H, et al. Extreme-ultraviolet phase-shifting point-diffraction interferometer: a wave-front metrology tool with subangstrom reference-wave accuracy [J]. Applied Optics, 1999, 38(35): 7252-7263.
- [18] Sugisaki K, Hasegawa M, Okada M, et al. EUVA's challenges toward 0.1 nm accuracy in EUV at-wavelength interferometry [M]. Berlin: Springer, 2006: 252-266.
- [19] Murakami K, Saito J, Ota K, et al. Development of an experimental EUV interferometer for benchmarking several EUV wavefront metrology schemes [J]. Proceedings of SPIE, 2003, 5037: 257-264.
- [20] Hasegawa T, Ouchi C, Hasegawa M, et al. EUV wavefront metrology system in EUVA [J]. Proceedings of SPIE, 2004, 5374: 797.
- [21] Feng P, Tang F, Wang X Z, et al. Dual-fiber point diffraction interferometer to measure the wavefront aberration of an imaging system[J]. Applied Optics, 2020, 59(10): 3093-3096.
- [22] Dong G J, Tang F, Wang X Z, et al. Study on high precision magnification measurement of imaging systems [J]. Acta Optica Sinica, 2018, 38 (7): 0712007. 董冠极, 唐峰, 王向朝, 等. 成像系统倍率高精度测量技术研究[J]. 光学学报, 2018, 38(7): 0712007.
- [23] Goldberg K A. Extreme ultraviolet interferometry [R]. Berkeley: Lawrence Berkeley National Lab (LBNL), 1997: 69-76.
- [24] Evans C J. PVr-a robust amplitude parameter for optical surface specification[J]. Optical Engineering, 2009, 48(4): 043605.

Dual-Hole Point Diffraction Interferometer for Measuring the Wavefront Aberration of an Imaging System

Feng Peng^{1,2}, Tang Feng^{1,2*}, Wang Xiangzhao^{1,2}, Lu Yunjun^{1,2}, Xu Jinghao¹, Guo Fudong¹, Zhang Guoxian¹

¹ Laboratory of Information Optics and Opto-Electronic Technology, Shanghai Institute of Optics and Fine Mechanics, Chinese Academy of Sciences, Shanghai 201800, China;

² Center of Materials Science and Optoelectronics Engineering, University of Chinese Academy of Sciences, Beijing 100049, China

Abstract

Objective Wavefront aberration describes the properties of a small-aberration imaging optical system. In a high-quality microscope objective lens and space telescope, the wavefront errors should be within $\lambda/14$ RMS (where λ is the operational wavelength and RMS is the root mean square value). To meet required wavefront quality of the optical systems for extreme ultraviolet lithography, the error must be less than 0.45 nm RMS. Therefore, wavefront measurements are highly demanded. At present, wavefronts are typically measured by Hartmann sensors, Fizeau interferometers, Twyman-Green interferometers, shearing interferometry, or point-diffraction interferometry. The Shark-Hartmann sensor covers a large measurement range and can quickly measure the wavefront, but with lower resolution than interferometry. The Fizeau and Twyman-Green interferometers cannot measure to higher accuracy than their standard lenses, and cannot be installed in systems with limited space.

In the present study, we report a phase-shifting point-diffraction interferometer with several advantages: high optical field uniformity, high measurable numerical aperture, and a quasi-common optical path. The optical signals are transmitted through single-mode fibers that improve the flexibility of the interferometer system. Our results are anticipated to assist wavefront-aberration detection in high-precision photolithographic projection lenses.

Methods We developed a dual-hole point diffraction interferometer (DHPDI) based on a dual-fiber optical path. First, we designed the measuring principle of the interferometer. The interferometer uses a diode-pumped solid-state laser with multi-longitudinal modes. The laser operating wavelength is 532 nm and the coherence length is several centimeters. The two laser beams form a quasi-common optical path interferometer structure. The intensities of the beams are controlled by interference arms connected with adjustable attenuators, one of which is connected to a phase shifter. The two single-mode optical fibers of the object surface output two beams of coherent

light. The end faces are imaged by the lens at two pinholes of the object surface mask, and are filtered by the pinholes to form two standard spherical-wavefront illumination imaging systems. One wavefront becomes the measurement wavefront and the other becomes the reference wavefront through the imaging system to be measured. The two beams overlap and produce an interference pattern at a charge-coupled device camera. The wavefront phase map is measured using a phase-shifting method. In the experiments, a DHPDI and a dual-fiber point-diffraction interferometer (DFPDI) were set up to detect the same projection objective lens. The experimental results were analyzed and the measurement results of both interferometers were compared to verify the effectiveness of the DHPDI.

Results and Discussions This paper proposes our DHPDI for measuring wavefront aberrations of imaging systems. Its advantages are high optical field uniformity, a high measurable numerical aperture, a quasi-common optical path, and a phase-shift element besides the imaging optical path of the system (Fig. 1). The DHPDI is designed with two measurement modes: point-diffraction measurement mode and system-errors measurement mode (Fig. 2). In point-diffraction mode, the DHPDI measures the geometric optical path error and detector tilt error of the test light and point-diffraction light, which mainly appear as coma aberration and astigmatism, respectively. These geometric optical path differences can be quickly and conveniently calibrated in system-errors mode. Both measurement modes can be used together for high-precision detection of wave aberrations in the imaging system. We constructed a DHPDI system that measures the wavefront aberration of a $5 \times$ demagnification projection objective lens with a numerical aperture of 0.3, and supplied it with a 532 nm laser (see Methods for laser details). The DHPDI was verified in experiments (Figs. 3 and 4), and its results were compared with those of the DFPDI (Figs. 5–7). The experimental results confirmed the theoretical deviation. When detecting the wavefront aberrations of the same projection objective lens, both measurement methods gave nearly consistent wavefront distributions, with a relative error of 0.07 nm RMS.

Conclusions We have demonstrated an advanced DHPDI. With a pinhole diameter of 700 nm, the deviation of the diffracted wavefront from spherical meets the requirements of wave aberration detection in high-precision imaging systems. The optical signals are transmitted through single-mode fibers, enabling a flexible interferometer system. The DHPDI also allows convenient adjustment of the interference contrast and phase-shifting outside the imaging optical path.

We then constructed DHPDI and DFPDI systems for measuring the wavefront aberration of a $5 \times$ projection objective lens with a numerical aperture of 0.3. In both modes, the contrast in the interferogram exceeded 65%. Moreover, the intensity uniformity of the interferogram in DHPDI was approximately twice that in DFPDI. Such uniform intensity can improve the accuracy of pupil-edge detection. The relative error of the wavefront distribution of the two detection results is less than 0.1 nm RMS, and the theoretical deviation was verified in the experiments.

Key words measurement; point diffraction; pinhole point diffraction; wave aberration detection; interferometry

OCIS codes 120.3180; 120.4640; 120.5050